*Journal of Sound and Vibration* (1997) **203**(3), 389–408

# NON-LINEAR BEARING STIFFNESS PARAMETER EXTRACTION FROM RANDOM RESPONSE IN FLEXIBLE ROTOR-BEARING SYSTEMS

R. TIWARI AND N. S. VYAS

*Department of Mechanical Engineering, Indian Institute of Technology, Kanpur, India*

(*Received* 20 *July* 1995, *and in final form* 17 *September* 1996)

A procedure for estimation of non-linear stiffness parameters of rolling element bearings supporting a flexible rotor, based on analysis of the random response signals picked up from the bearing caps, is developed. The non-linear multi-degree-of-freedom equations, governing the motion of a flexible shaft carrying a disc and experiencing random excitations due to imperfections of the bearing surfaces and assembly, are subjected to co-ordinate transformation and subsequently modelled as multi-dimensional Markov process through the Fokker–Planck equation. The solution procedure for the Fokker–Planck equation and the assumptions involved are outlined. The vibrations experienced at the bearings are processed through a curve fitting algorithm to obtain the necessary bearing stiffness parameters. The technique has an advantage over other existing ones in that it does not require an estimate of the excitation forces and measurements of vibrations at the rotor disc and works directly on the response signals from the bearing caps. The algorithm is illustrated for a laboratory rotor–bearing test rig and the result are compared with those obtained through an existing analytical model. The developed algorithm is tested by numerical simulation.



## 1. INTRODUCTION

Estimation of bearing stiffness parameters is crucial to rotor designs. Stiffness estimation involves establishing a relationship between the load carried by the bearing and its deformation. The classical solution for the local stress and deformation of two elastic bodies apparently in contact at a single point was established by Hertz [1]. The early studies [2, 3] on bearings concern vibrations caused due to geometric imperfections of contact surfaces. Honrath [4] and Elsermans *et al*. [5] examined the stiffness and damping of rolling element bearings experimentally. Theoretical models [6, 7] are available for estimation of bearing stiffness under static loading conditions. A method for determination of the non-linear characteristics of bearings using the procedure of Krylov–Bogoliubov–Mitropolsky has been suggested by Kononenko and Plakhtienko [8]. Walford and Stone [9] designed and fabricated a test rig for direct measurement of the relative displacement of the shaft and bearing housing for the oscillating force applied to the bearing housing, which is used to obtain the stiffness parameters. Comprehensive investigations have been carried out on the high frequency response of bearings [10] and its relation to surface irregularities [11–13]. Kraus *et al*. [14] presented a method for the extraction of rolling element bearing stiffness and damping under operating conditions. The method is based on experimental modal analysis combined with a mathematical model of the rotor–bearing–support system. The method is applied for investigation of the effect of speed, pre-load and free outer race bearings on stiffness and damping. Muszynska [15] has

0022–460X/97/230389 + 20 $25.00/0/sv960786 

developed a perturbation technique for estimation of these parameters. The technique involves a controlled input excitation to be given to the bearings. Goodwin [16] reviewed the experimental approaches to rotor support impedance measurement. Non-linear stochastic contact vibrations and friction at a Hertzian contact have been studied by Hess *et al*. [17]. The experimentation involves excitation of the bearings either externally by a white Gaussian random normal load or within the contact region by a rough surface input and the analytical approach is based on the solution of the Fokker–Planck equation. Lim and Singh [18] have analyzed the vibration transmission through rolling element bearings and effect of distributed contact load on roller bearing stiffness.

Recently, Tiwari and Vyas [19] proposed a technique for estimation of non-linear stiffness of rolling element bearing in rigid rotor–bearing systems, based on analysis of the random response signals picked up from the bearing caps. The governing non-linear single-degree-of-freedom equation with a random excitation force, resulting due to random imperfections of the bearing surfaces and assembly was modelled as one-dimensional Markov process through the Fokker–Planck equation. The solution of the Fokker–Planck equation was further processed to obtain the linear and non-linear bearing stiffness parameters. The technique has an advantage over other existing ones in that it does not require an estimate of the excitation forces and works directly on the response signals from the bearing caps.

The present study attempts to solve the problem of bearing stiffness parameter estimation for flexible rotors. In contrast to the rigid rotor case, which could be treated as a single-degree-of-freedom problem, the flexible rotor analysis becomes far more involved, for it poses a non-linear multi-degree-of-freedom case. The problem has been formulated for bending vibrations of a flexible shaft carrying a centrally located rigid disc and supported at the ends in non-linear bearings. Torsional modes of rotating machinery generally occur at speeds much higher than the bending criticals. Coupling between bending and torsion can occur in machinery involving elements such as flexible couplings between driving and driven units [20]. Torsional stiffness of the shaft is not accounted for in the present formulation. The procedure developed is illustrated for rotors supported in rolling element ball bearings, for which cross-coupled stiffness effects are weak and can be ignored. The excitation to the balanced system is taken to be random in nature, primarily arising out of bearing and assembly imperfections. The inverse problem of parameter estimation is approached by initially effecting a co-ordinate transformation. This transformation allows the governing equations to be modelled as multi-dimensional Markov processes through the Fokker–Planck equations. The solution to the Fokker–Planck equation is obtained under certain engineering assumptions. A curve fitting algorithm is developed to process the statistical response of the system obtained by the solution of the Fokker–Planck equation to extract the rotor–bearing stiffness parameters. The procedure is illustrated for a laboratory test rig and the experimental results are compared with the analytical guidelines of Harris and Ragulskis [6, 7]. The algorithm developed is tested by the Monte Carlo numerical simulation procedure.

## 2. EQUATIONS OF MOTION

A balanced rotor, with a centrally located disc on a massless flexible shaft supported in bearings at the ends, is shown in Figure 1. The shaft is treated as a free–free body, carrying unknown effective bearing masses $m_1$ and $m_2$ at its ends and the known disc mass $m_3$ in the center. The bearings are incorporated through external "forces", $F_b$, acting on masses $m_1$ and $m_2$. Taking the shaft stiffness and damping forces as $F_s$ and $F_d$, respectively,

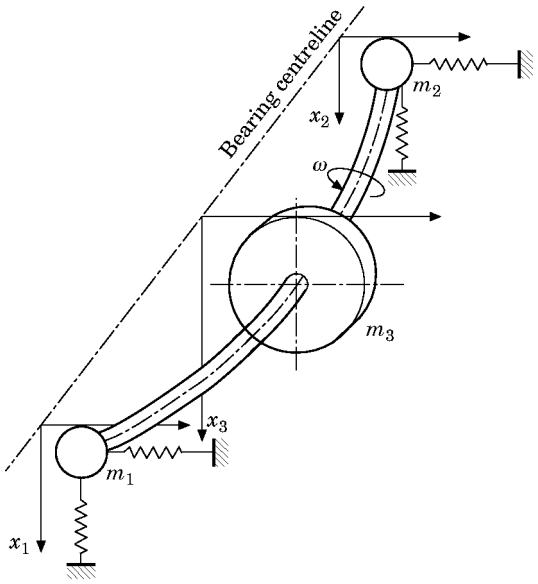


Figure 1. A flexible rotor on rolling element bearings.

the equations of motion are written as (the problem formulation in the horizontal direction remains identical to that in the vertical direction)

$$-F_{d_1} - F_{s_1} - F_{b_1} = m_1\ddot{x}_1, \qquad -F_{d_2} - F_{s_2} - F_{b_2} = m_2\ddot{x}_2, \qquad -F_{d_3} - F_{s_3} = m_3\ddot{x}_3. \quad (1\text{–}3)$$

The shaft stiffness forces are

$$F_{s_1} = (k_{11}x_1 + k_{12}x_2 + k_{13}x_3), \qquad F_{s_2} = (k_{12}x_1 + k_{22}x_2 + k_{23}x_3),$$
$$F_{s_3} = (k_{13}x_1 + k_{23}x_2 + k_{33}x_3). \quad (4)$$

The shaft stiffness parameter $k_{ij}$ is defined as the $i$th force corresponding to a unit $j$ deflection with all other deflections held to zero and can be obtained from strength of materials formulae.

The shaft damping forces are

$$F_{d_1} = \alpha_{11}\dot{x}_1 + \alpha_{12}\dot{x}_2 + \alpha_{13}\dot{x}_3, \qquad F_{d_2} = \alpha_{12}\dot{x}_1 + \alpha_{22}\dot{x}_2 + \alpha_{23}\dot{x}_3,$$
$$F_{d_3} = \alpha_{13}\dot{x}_1 + \alpha_{23}\dot{x}_2 + \alpha_{33}\dot{x}_3. \quad (5)$$

The shaft damping parameter, $\alpha_{ij}$, can be defined in a manner similar to $k_{ij}$.

The excitation to the system is taken to be random in nature. The bearing surface imperfections, caused by the random deviations from their standard theoretical design and progressive surface and subsurface deteriorations, are large enough to cause measurable levels of vibration and can be the primary source of these excitations. In addition, excitation can arise from inaccuracies in the rotor–bearing–housing assembly etc. Taking $s_1$ and $s_2$ as the effective random displacements at the bearings, primarily due to surface imperfections and inaccuracies in the rotor–bearing–housing assembly, the bearing forces on masses $m_1$ and $m_2$ can be written as

$$F_{b_1} = \{k_{L_1}(x_1 - s_1) + k_{NL_1}G(x_1 - s_1)\}, \qquad F_{b_2} = \{k_{L_2}(x_2 - s_2) + k_{NL_2}G(x_2 - s_2)\} \quad (6)$$

In the above, $k_L$ and $k_{NL}$ are the unknown linear and non-linear bearing stiffness parameters and $G$ can be a polynomial in $x$.

Equations (6) can be rewritten, more generally, as

$$F_{b_1} = \{k_{L_1}x_1 + k_{NL_1}G(x_1)\} - F_1(t), \qquad F_{b_2} = \{k_{L_2}x_2 + k_{NL_2}G(x_2)\} - F_2(t), \tag{7}$$

where $F_1(t)$ and $F_2(t)$ are the random components of the bearing forces.

Using equations (4), (5) and (7) the equations of motion (1)–(3) can be written as [21, 22]

$$\begin{bmatrix} m_1 & 0 & 0 \\ 0 & m_2 & 0 \\ 0 & 0 & m_3 \end{bmatrix}\begin{Bmatrix} \ddot{x}_1 \\ \ddot{x}_2 \\ \ddot{x}_3 \end{Bmatrix} + \begin{bmatrix} \alpha_{11} & \alpha_{12} & \alpha_{13} \\ \alpha_{12} & \alpha_{22} & \alpha_{23} \\ \alpha_{13} & \alpha_{23} & \alpha_{33} \end{bmatrix}\begin{Bmatrix} \dot{x}_1 \\ \dot{x}_2 \\ \dot{x}_3 \end{Bmatrix} + \begin{Bmatrix} \partial V(x_1, x_2, x_3)/\partial x_1 \\ \partial V(x_1, x_2, x_3)/\partial x_2 \\ \partial V(x_1, x_2, x_3)/\partial x_3 \end{Bmatrix} = \begin{Bmatrix} F_1 \\ F_2 \\ 0 \end{Bmatrix}, \tag{8}$$

where

$$V(x_1, x_2, x_3) = m_3[\tfrac{1}{2}\omega_{11}^2 x_1^2 + \tfrac{1}{2}\omega_{22}^2 x_2^2 + \tfrac{1}{2}\omega_{33}^2 x_3^2 + \omega_{12}^2 x_1 x_2 + \omega_{23}^2 x_2 x_3 + \omega_{13}^2 x_1 x_3] + m_3[\tfrac{1}{2}\omega_{n_1}^2 x_1^2 + \omega_{n_1}^2 \lambda_1 g(x_1) + \tfrac{1}{2}\omega_{n_2}^2 x_2^2 + \omega_{n_2}^2 \lambda_2 g(x_2)], \tag{9}$$

$$g(x) = \int_0^x G(\xi)\, \mathrm{d}\xi, \tag{10}$$

$$\omega_{ij}^2 = k_{ij}/m_3, \qquad \omega_{n_i}^2 = k_{L_i}/m_3, \qquad \lambda_i = k_{NL_i}/\omega_{n_i}^2 m_3. \tag{11}$$

The Markov vector approach extended to non-linear multi-degree-of-freedom systems [23] is adopted for the solution of equations (8)

The equations of motion (8) with damping and forces $F_1$ and $F_2$ set to zero, are solved for eigenvalues $p_1^2$, $p_2^2$, $p_3^2$ and the orthonormal modal matrix $[U]$, so that

$$[U]^{\mathrm{T}}\begin{bmatrix} k_{11} & k_{12} & k_{13} \\ k_{12} & k_{22} & k_{23} \\ k_{13} & k_{23} & k_{33} \end{bmatrix}[U] = \begin{bmatrix} p_1^2 & 0 & 0 \\ 0 & p_2^2 & 0 \\ 0 & 0 & p_3^2 \end{bmatrix}, \tag{12}$$

$$[U]^{\mathrm{T}}\begin{bmatrix} m_1 & 0 & 0 \\ 0 & m_2 & 0 \\ 0 & 0 & m_3 \end{bmatrix}[U] = \begin{bmatrix} 1 & 0 & 0 \\ 0 & 1 & 0 \\ 0 & 0 & 1 \end{bmatrix}. \tag{13}$$

(The eigenvalue and eigenvector matrix elements are given in Appendix A.)

Application of the co-ordinate transformation

$$\begin{Bmatrix} x_1 \\ x_2 \\ x_3 \end{Bmatrix} = [U]\begin{Bmatrix} \eta_1 \\ \eta_2 \\ \eta_3 \end{Bmatrix} \tag{14}$$

to the equations of motion (8) yields

$$\begin{bmatrix} 1 & 0 & 0 \\ 0 & 1 & 0 \\ 0 & 0 & 1 \end{bmatrix}\begin{Bmatrix} \ddot{\eta}_1 \\ \ddot{\eta}_2 \\ \ddot{\eta}_3 \end{Bmatrix} + \begin{bmatrix} \beta_{11} & 0 & 0 \\ 0 & \beta_{22} & 0 \\ 0 & 0 & \beta_{33} \end{bmatrix}\begin{Bmatrix} \dot{\eta}_1 \\ \dot{\eta}_2 \\ \dot{\eta}_3 \end{Bmatrix} + \begin{Bmatrix} (1/M_1)\, \partial V(\eta_1, \eta_2, \eta_3)/\partial \eta_1 \\ (1/M_2)\, \partial V(\eta_1, \eta_2, \eta_3)/\partial \eta_{21} \\ (1/M_3)\, \partial V(\eta_1, \eta_2, \eta_3)/\partial \eta_3 \end{Bmatrix} = \begin{Bmatrix} q_1 \\ q_2 \\ q_3 \end{Bmatrix}, \tag{15}$$

where

$$\begin{bmatrix} \beta_{11} & 0 & 0 \\ 0 & \beta_{22} & 0 \\ 0 & 0 & \beta_{33} \end{bmatrix} = [U]^{\mathrm{T}} \begin{bmatrix} \alpha_{11} & \alpha_{12} & \alpha_{13} \\ \alpha_{12} & \alpha_{22} & \alpha_{23} \\ \alpha_{13} & \alpha_{23} & \alpha_{33} \end{bmatrix} [U], \tag{16}$$

$$\begin{aligned} V(\eta_1, \eta_2, \eta_3) = m_3 \, & [\tfrac{1}{2}\omega_{11}^2(\eta_1 + u_{31}\eta_2 + u_{21}\eta_3)^2 + \tfrac{1}{2}\omega_{22}^2(\eta_1 + u_{32}\eta_2 + u_{22}\eta_3)^2 \\ & + \tfrac{1}{2}\omega_{33}^2(\eta_1 + \eta_2 + \eta_3)^2 + \omega_{12}^2(\eta_1 + u_{31}\eta_2 + u_{21}\eta_3)(\eta_1 + u_{32}\eta_2 + u_{22}\eta_3) \\ & + \omega_{23}^2(\eta_1 + u_{32}\eta_2 + u_{22}\eta_3)(\eta_1 + \eta_2 + \eta_3) + \omega_{13}^2(\eta_1 + u_{31}\eta_2 + u_{21}\eta_3) \\ & \times (\eta_1 + \eta_2 + \eta_3)] + m_3[\tfrac{1}{2}\omega_{n_1}^2(\eta_1 + u_{31}\eta_2 + u_{21}\eta_3)^2 \\ & + \omega_{n_1}^2\lambda_1 g(\eta_1 + u_{31}\eta_2 + u_{21}\eta_3) + \tfrac{1}{2}\omega_{n_2}^2(\eta_1 + u_{32}\eta_2 + u_{22}\eta_3)^2 \\ & + \omega_{n_2}^2\lambda_2 g(\eta_1 + u_{32}\eta_2 + u_{22}\eta_3)], \end{aligned} \tag{17}$$

$$\begin{Bmatrix} q_1 \\ q_2 \\ q_3 \end{Bmatrix} = [U]^{\mathrm{T}} \begin{Bmatrix} F_1 \\ F_2 \\ 0 \end{Bmatrix}. \tag{18}$$

The modal masses $M_1$, $M_2$ and $M_3$ are given by

$$M_1 = m_1 + m_2 + m_3, \qquad M_2 = u_{31}^2 m_1 + m_2 + u_{32}^2 m_3, \qquad M_3 = u_{21}^2 m_1 + m_2 + u_{22}^2 m_3.$$

## 3. RESPONSE

The approach to obtaining the response of the system is greatly simplified if the random excitation to the system is assumed to be such that the generalized forces, $q_i$, in equations (15) can be treated as ideal white noise. Many engineering applications are based on this idealization, and it turns out that the responses obtained through such models are quite acceptable if the time scale of the excitation is much smaller than the time scale of the response [24]. The time scale of the excitation is the correlation time, roughly defined as the length of time separation beyond which excitation process is nearly uncorrelated. The time scale of the response is the measure of the memory duration of the system, which is generally about one-quarter of the natural period of a mode that contributes significantly to the response. The excitation of equation (15) is treated as uncorrelated Gaussian, white random forces with the following properties:

$$E[q_1(t)] = 0, \qquad E[q_2(t)] = 0, \qquad E[q_3(t)] = 0,$$

$$E[q_1(t_1)q_1(t_2)] = 2\pi\phi_1\delta(t_2 - t_1), \qquad E[q_2(t_1)q_2(t_2)] = 2\pi\phi_2\delta(t_2 - t_1),$$

$$E[q_3(t_1)q_3(t_2)] = 2\pi\phi_3\delta(t_2 - t_1), \tag{19}$$

where $\phi_1$, $\phi_2$ and $\phi_3$ denote the excitation intensity factors and $\delta(t_2 - t_1)$ is the Dirac delta function.

The joint probability density function, $p(\eta_1, \eta_2, \eta_3, \dot{\eta}_1, \dot{\eta}_2, \dot{\eta}_3)$, for the motion governed by equations (15) and excitation with properties described by equations (19) can be described by the Fokker–Planck equation [25]

$$-\dot{\eta}_1 \frac{\partial p}{\partial \eta_1} - \frac{1}{M_1}\frac{\partial V}{\partial \eta_1}\frac{\partial p}{\partial \dot{\eta}_1} + \frac{\partial}{\partial \dot{\eta}_1}\left(\beta_{11}\dot{\eta}_1 p + \pi\phi_1 \frac{\partial p}{\partial \dot{\eta}_1}\right) - \dot{\eta}_2 \frac{\partial p}{\partial \eta_2} - \frac{1}{M_2}\frac{\partial V}{\partial \eta_2}\frac{\partial p}{\partial \dot{\eta}_2}$$

$$+\frac{\partial}{\partial \dot{\eta}_2}\left(\beta_{22}\dot{\eta}_2 p + \pi\phi_2 \frac{\partial p}{\partial \dot{\eta}_2}\right) - \dot{\eta}_3 \frac{\partial p}{\partial \eta_3} - \frac{1}{M_3}\frac{\partial V}{\partial \eta_3}\frac{\partial p}{\partial \dot{\eta}_3} + \frac{\partial}{\partial \dot{\eta}_3}\left(\beta_{33}\dot{\eta}_3 p + \pi\phi_3 \frac{\partial p}{\partial \dot{\eta}_3}\right) = \frac{\partial p}{\partial t}. \tag{20}$$

For a stationary case, equation (20) is reduced to

$$-\dot{\eta}_1 \frac{\partial p}{\partial \eta_1} - \frac{1}{M_1}\frac{\partial V}{\partial \eta_1}\frac{\partial p}{\partial \dot{\eta}_1} + \frac{\partial}{\partial \dot{\eta}_1}\left(\beta_{11}\dot{\eta}_1 p + \pi\phi_1 \frac{\partial p}{\partial \dot{\eta}_1}\right) - \dot{\eta}_2 \frac{\partial p}{\partial \eta_2} - \frac{1}{M_2}\frac{\partial V}{\partial \eta_2}\frac{\partial p}{\partial \dot{\eta}_2}$$

$$+\frac{\partial}{\partial \dot{\eta}_2}\left(\beta_{22}\dot{\eta}_2 p + \pi\phi_2 \frac{\partial p}{\partial \dot{\eta}_2}\right) - \dot{\eta}_3 \frac{\partial p}{\partial \eta_3} - \frac{1}{M_3}\frac{\partial V}{\partial \eta_3}\frac{\partial p}{\partial \dot{\eta}_3} + \frac{\partial}{\partial \dot{\eta}_3}\left(\beta_{33}\dot{\eta}_3 p + \pi\phi_3 \frac{\partial p}{\partial \dot{\eta}_3}\right) = 0. \tag{21}$$

With the assumption [22]

$$\left(\frac{\beta_{11}}{M_1\phi_1}\right) = \left(\frac{\beta_{22}}{M_2\phi_2}\right) = \left(\frac{\beta_{33}}{M_3\phi_3}\right) = \gamma,$$

equation (21) can be solved to obtain the joint probability density of displacements and velocities in terms of the transformed co-ordinate system as [25]

$$p(\eta_1, \eta_2, \eta_3, \dot{\eta}_1, \dot{\eta}_2, \dot{\eta}_3) = c\,\exp\left[-\frac{\gamma}{\pi}\{M_1\dot{\eta}_1^2 + M_2\dot{\eta}_2^2 + M_3\dot{\eta}_3^2 + V(\eta_1, \eta_2, \eta_3)\}\right]. \tag{22}$$

Performing the inverse orthonormal transformation and noting that the term $M_1\dot{\eta}_1^2 + M_2\dot{\eta}_2^2 + M_3\dot{\eta}_3^2 + V(\eta_1\eta_2\eta_3)$ on the right side of equation (22) represents the total kinetic and potential energy of the system and that $\gamma$ is a constant, the joint probability density of displacements and velocities in the original set of co-ordinates is

$$p(x_1, x_2, x_3, \dot{x}_1, \dot{x}_2, \dot{x}_3) = c\,\exp\left[-\frac{\gamma}{\pi}\{m_1\dot{x}_1^2 + m_2\dot{x}_2^2 + m_3\dot{x}_3^2 + V(x_1, x_2, x_3)\}\right]. \tag{23}$$

The joint probability functions $p(x_1, x_2, x_3)$ and $p(\dot{x}_1, \dot{x}_2, \dot{x}_3)$ are obtained from equation (23) as [26]

$$p(x_1, x_2, x_3) = \int_{-\infty}^{\infty}\int_{-\infty}^{\infty}\int_{-\infty}^{\infty} p(x_1, x_2, x_3, \dot{x}_1, \dot{x}_2, \dot{x}_3)\,\mathrm{d}\dot{x}_1\,\mathrm{d}\dot{x}_2\,\mathrm{d}\dot{x}_3$$

$$= c_1\,\exp\left[-\frac{\gamma}{\pi}V(x_1, x_2, x_3)\right], \tag{24}$$

with

$$c_1 = 1 \Big/ \int_{-\infty}^{\infty} \int_{-\infty}^{\infty} \int_{-\infty}^{\infty} \exp\left[ -\frac{\gamma}{\pi} V(x_1, x_2, x_3) \right] \mathrm{d}x_1 \, \mathrm{d}x_2 \, \mathrm{d}x_3$$

and

$$p(\dot{x}_1, \dot{x}_2, \dot{x}_3) = \int_{-\infty}^{\infty} \int_{-\infty}^{\infty} \int_{-\infty}^{\infty} p(x_1, x_2, x_3, \dot{x}_1, \dot{x}_2, \dot{x}_3) \, \mathrm{d}x_1 \, \mathrm{d}x_2 \, \mathrm{d}x_3$$

$$= \left[ \frac{1}{\pi} \sqrt{\frac{\gamma}{2}} \right]^3 \sqrt{m_1 m_2 m_3} \exp\left[ -\frac{\gamma}{\pi} \left\{ \tfrac{1}{2} (m_1 \dot{x}_1^2 + m_2 \dot{x}_2^2 + m_3 \dot{x}_3^2) \right\} \right]. \tag{25}$$

The joint probability function $p(x_1, x_2)$ is obtained as

$$p(x_1, x_2) = \int_{-\infty}^{\infty} p(x_1, x_2, x_3) \, \mathrm{d}x_3$$

$$= \int_{-\infty}^{\infty} c_1 \exp\left[ -\frac{\gamma}{\pi} \left\{ V(x_1, x_2, x_3) \right\} \right] \mathrm{d}x_3$$

$$= c_2 \exp\left[ -\frac{m_3 \gamma}{\pi} \left\{ \tfrac{1}{2} \left( \omega_{11}^2 + \omega_{n_1}^2 - \frac{\omega_{13}^4}{\omega_{33}^2} \right) x_1^2 + \tfrac{1}{2} \left( \omega_{22}^2 + \omega_{n_2}^2 - \frac{\omega_{23}^4}{\omega_{33}^2} \right) x_2^2 \right. \right.$$

$$\left. \left. + \left( \omega_{12}^2 - \frac{\omega_{13}^2 \omega_{23}^2}{\omega_{33}^2} \right) x_1 x_2 + (\omega_{n_1}^2 \lambda_1) g(x_1) + (\omega_{n_2}^2 \lambda_2) g(x_2) \right\} \right], \tag{26}$$

with

$$c_2 = \left( \frac{\pi}{\omega_{33}} \sqrt{\frac{2}{m_3 \gamma}} \right) \Big/ \int_{-\infty}^{\infty} \int_{-\infty}^{\infty} \int_{-\infty}^{\infty} \exp\left[ -\frac{\gamma}{\pi} V(x_1, x_2, x_3) \right] \mathrm{d}x_1 \, \mathrm{d}x_2 \, \mathrm{d}x_3.$$

The probability density functions $p(\dot{x}_1)$ and $p(\dot{x}_2)$ are as follows:

$$p(\dot{x}_1) = \int_{-\infty}^{\infty} \int_{-\infty}^{\infty} p(\dot{x}_1, \dot{x}_2, \dot{x}_3) \, \mathrm{d}\dot{x}_2 \, \mathrm{d}\dot{x}_3$$

$$= \left[ \frac{1}{\pi} \sqrt{\frac{m_1 \gamma}{2}} \right] \exp\left[ -\frac{\gamma}{\pi} \left\{ \frac{1}{2} m_1 \dot{x}_1^2 \right\} \right], \tag{27}$$

$$p(\dot{x}_2) = \int_{-\infty}^{\infty} \int_{-\infty}^{\infty} p(\dot{x}_1, \dot{x}_2, \dot{x}_3) \, \mathrm{d}\dot{x}_1 \, \mathrm{d}x_3$$

$$= \left[ \frac{1}{\pi} \sqrt{\frac{m_2 \gamma}{2}} \right] \exp\left[ -\frac{\gamma}{\pi} \left\{ \frac{1}{2} m_2 \dot{x}_2^2 \right\} \right]. \tag{28}$$

The variances of the velocity responses $\dot{x}_1$ and $\dot{x}_2$ are obtained as follows:

$$\sigma_{\dot{x}_1}^2 = \int_{-\infty}^{\infty} \dot{x}_1^2 p(\dot{x}_1)\,\mathrm{d}x_1 = \pi/m_1\gamma, \tag{29}$$

$$\sigma_{\dot{x}_2}^2 = \int_{-\infty}^{\infty} \dot{x}_2^2 p(\dot{x}_2)\,\mathrm{d}\dot{x}_2 = \pi/m_2\gamma. \tag{30}$$

Combining equations (29) and (30),

$$\sigma_{\dot{x}_1}\sigma_{\dot{x}_2} = \frac{\pi}{\gamma}\frac{1}{\sqrt{m_1 m_2}}. \tag{31}$$

The joint probability density function for the displacement responses $x_1$ and $x_2$, from equations (26) and (31), can be written as

$$p(x_1, x_2) = c_2 \exp\left[ -\frac{\sqrt{\mu_1\mu_2}}{\sigma_{\dot{x}_1}\sigma_{\dot{x}_2}} \left\{ \tfrac{1}{2}\left(\omega_{11}^2 + \omega_{n_1}^2 - \frac{\omega_{13}^4}{\omega_{33}^2}\right)x_1^2 + \tfrac{1}{2}\left(\omega_{22}^2 + \omega_{n_2}^2 - \frac{\omega_{23}^4}{\omega_{33}^2}\right)x_2^2 \right.\right.$$

$$\left.\left. + \left(\omega_{12}^2 - \frac{\omega_{13}^2\omega_{23}^2}{\omega_{33}^2}\right)x_1x_2 + (\omega_{n_1}^2\lambda_1)g(x_1) + (\omega_{n_2}^2\lambda_2)g(x_2) \right\} \right],$$

with

$$c_2 = \left(\frac{\pi}{\omega_{33}}\sqrt{\frac{2}{m_3\gamma}}\right) \Big/ \int_{-\infty}^{\infty}\int_{-\infty}^{\infty}\int_{-\infty}^{\infty} \exp\left[ -\frac{\sqrt{\mu_1\mu_2}}{m_3\sigma_{\dot{x}_1}\sigma_{\dot{x}_2}} V(x_1, x_2, x_3) \right] \mathrm{d}x_1\,\mathrm{d}x_2\,\mathrm{d}x_3,$$

$$\mu_1 = m_3/m_1, \qquad \mu_2 = m_3/m_2. \tag{32}$$

## 4. EXTRACTION OF BEARING PARAMETERS

The bearing parameters are obtained from the experimentally obtained random response in terms of the linear stiffness parameters $\omega_{n_1}^2$ and $\omega_{n_2}^2$, the non-linear stiffness parameters $\lambda_1$ and $\lambda_2$, and the disc–bearing mass ratios $\mu_1$ and $\mu_2$. These parameters are obtained for both the vertical and horizontal directions, with the problem formulation, in the horizontal direction, remaining identical to that in the vertical direction.

The joint probability density function $p(x_1, x_2)$ for a set of displacements $(x_{1_i}, x_{2_j})$ $(x_{1_{(i+1)}}, x_{2_{(j+1)}})$, ($x_{1_{(i+1)}} > x_{1_i}$ and $x_{2_{(j+1)}} > x_{2_j}$), from equation (32) are as follows:

$$p(x_{1_i}, x_{2_j}) = c_2 \exp\left[ -\frac{\sqrt{\mu_1\mu_2}}{\sigma_{\dot{x}_1}\sigma_{\dot{x}_2}} \left\{ \tfrac{1}{2}\left(\omega_{11}^2 + \omega_{n_1}^2 - \frac{\omega_{13}^4}{\omega_{33}^2}\right)x_{1_i}^2 + \tfrac{1}{2}\left(\omega_{22}^2 + \omega_{n_2}^2 - \frac{\omega_{23}^4}{\omega_{33}^2}\right)x_{2_j}^2 \right.\right.$$

$$\left.\left. + \left(\omega_{12}^2 - \frac{\omega_{13}^2\omega_{23}^2}{\omega_{33}^2}\right)x_{1_i}x_{2_j} + (\omega_{n_1}^2\lambda_1)g(x_{1_i}) + (\omega_{n_2}^2\lambda_2)g(x_{2_j}) \right\} \right], \tag{33}$$

$$p(x_{1_{(i+1)}}, x_{2_{(j+1)}}) = c_2 \exp\Bigg[ -\frac{\sqrt{\mu_1\mu_2}}{\sigma_{\dot{x}_1}\sigma_{\dot{x}_2}} \Bigg\{ \tfrac{1}{2}\left(\omega_{11}^2 + \omega_{n_1}^2 - \frac{\omega_{13}^4}{\omega_{33}^2}\right) x_{1_{(i+1)}}^2$$

$$+ \tfrac{1}{2}\left(\omega_{22}^2 + \omega_{n_2}^2 - \frac{\omega_{23}^4}{\omega_{33}^2}\right) x_{2_{(j+1)}}^2 + \left(\omega_{12}^2 - \frac{\omega_{13}^2\omega_{23}^2}{\omega_{33}^2}\right) x_{1_{(i+1)}} x_{2_{(j+1)}}$$

$$+ (\omega_{n_1}^2\lambda_1) g(x_{1_{(i+1)}}) + (\omega_{n_2}^2\lambda_2) g(x_{2_{(j+1)}}) \Bigg\} \Bigg].$$

Defining

$$\Delta x_1 = x_{1_{(i+1)}} - x_{1_i}, \qquad \Delta x_2 = x_{2_{(j+1)}} - x_{2_j}$$

for small $\Delta x_1$ and $\Delta x_2$, one can write

$$p(x_{1_{(i+1)}}, x_{2_{(j+1)}}) = c_2 \exp\Bigg[ -\frac{\sqrt{\mu_1\mu_2}}{\sigma_{\dot{x}_1}\sigma_{\dot{x}_2}} \Bigg\{ \tfrac{1}{2}\left(\omega_{11}^2 + \omega_{n_1}^2 - \frac{\omega_{13}^4}{\omega_{33}^2}\right) x_{1_i}^2 + \tfrac{1}{2}\left(\omega_{22}^2 + \omega_{n_2}^2 - \frac{\omega_{23}^4}{\omega_{33}^2}\right) x_{2_j}^2$$

$$+ \left(\omega_{12}^2 - \frac{\omega_{13}^2\omega_{23}^2}{\omega_{33}^2}\right) x_{1_i} x_{2_j} + (\omega_{n_1}^2\lambda_1) g(x_{1_i}) + (\omega_{n_2}^2\lambda_2) g(x_{2_j}) \Bigg\} \Bigg]$$

$$\times \exp\Bigg[ -\frac{\sqrt{\mu_1\mu_2}}{\sigma_{\dot{x}_1}\sigma_{\dot{x}_2}} \Bigg\{ \left(\omega_{11}^2 + \omega_{n_1}^2 - \frac{\omega_{13}^4}{\omega_{33}^2}\right) (x_{1_i}\Delta x_1)$$

$$+ \left(\omega_{22}^2 + \omega_{n_2}^2 - \frac{\omega_{23}^4}{\omega_{33}^2}\right) (x_{2_j}\Delta x_2) + \left(\omega_{12}^2 - \frac{\omega_{13}^2\omega_{23}^2}{\omega_{33}^2}\right) (x_{1_i}\Delta x_2 + x_{2_j}\Delta x_1)$$

$$+ (\omega_{n_1}^2\lambda_1) G(x_{1_i})\Delta x + (\omega_{n_2}^2\lambda_2) G(x_{2_j})\Delta x_{2_1} \Bigg\} \Bigg]. \tag{34}$$

Combining equations (34) and (33) gives

$$p(x_{1_{(i+1)}}, x_{2_{(j+1)}}) = p(x_{1_i}, x_{2_j}) \exp\Bigg[ -\frac{\sqrt{\mu_1\mu_2}}{\sigma_{\dot{x}_1}\sigma_{\dot{x}_2}} \Bigg\{ \tfrac{1}{2}\left(\omega_{11}^2 + \omega_{n_1}^2 - \frac{\omega_{13}^4}{\omega_{33}^2}\right) (2x_{1_i}\Delta x_1)$$

$$+ \tfrac{1}{2}\left(\omega_{22}^2 + \omega_{n_2}^2 - \frac{\omega_{23}^4}{\omega_{33}^2}\right) (2x_{2_j}\Delta x_2) + \left(\omega_{12}^2 - \frac{\omega_{13}^2\omega_{23}^2}{\omega_{33}^2}\right) (x_{1_i}\Delta x_2 + x_{2_j}\Delta x_1)$$

$$+ (\omega_{n_1}^2\lambda_1) G(x_{1_i})\Delta x_1 + (\omega_{n_2}^2\lambda_2) G(x_{2_j})\Delta x_2 \Bigg\} \Bigg]. \tag{35}$$

For $N$ values of each displacement, $x_{1_i}, x_{1_2}, \ldots, x_{1_N}$, and $x_{2_1}, x_{2_2}, \ldots, x_{2_N}$, equation (35) can be expressed as a set of $(N-1)^2$ linear simultaneous algebraic equations, as

$$\left[\frac{\sigma_{\dot{x}_1}\sigma_{\dot{x}_2}}{\Delta x_1 \Delta x_2} \ln\left\{\frac{p(x_{1_i}, x_{2_j})}{p(x_{1_{(i+1)}}, x_{2_{(j+1)}})}\right\}\right]\left\{\frac{1}{\sqrt{\mu_1\mu_2}\omega_{n_1}^2}\right\} - \left[\frac{G(x_{1_i})}{\Delta x_2}\right]\{\lambda_1\} - \left[\frac{G(x_{2_j})}{\Delta x_1}\right]\left\{\frac{\lambda_2\omega_{n_2}^2}{\omega_{n_1}^2}\right\}$$

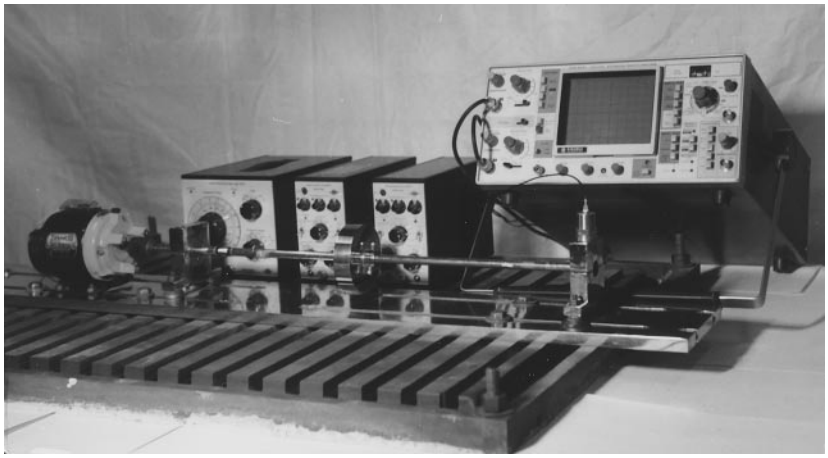

Figure 2. The rotor–bearing set-up.

$$+\left[\left(\frac{\omega_{13}^4}{\omega_{33}^2}-\omega_{11}^2\right)\left(\frac{x_{1_i}}{\Delta x_2}\right)+\left(\frac{\omega_{23}^4}{\omega_{33}^2}-\omega_{22}^2\right)\left(\frac{x_{2_j}}{\Delta x_1}\right)+\left(\frac{\omega_{13}^2\omega_{23}^2}{\omega_{33}^2}-\omega_{12}^2\right)\right.$$

$$\left.\times\left(\frac{x_{1_i}}{\Delta x_1}+\frac{x_{2_j}}{\Delta x_2}\right)\right]\left\{\frac{1}{\omega_{n_1}^2}\right\}+\left[\left(\frac{\omega_{23}^4}{\omega_{33}^2}-\omega_{11}^2\right)\left(\frac{x_{2_j}}{\Delta x_1}\right)\right]\left\{\frac{\left(1-\dfrac{\omega_{n_2}^2}{\omega_{n_1}^2}\right)}{\left(\dfrac{\omega_{23}^4}{\omega_{33}^2}-\omega_{22}^2\right)}\right\}=\left(\frac{x_{1_i}}{\Delta x_2}+\frac{x_{2_j}}{\Delta x_1}\right),$$

$$i=1,2,\ldots,(N-1),\qquad j=1,2,\ldots,(N-1). \tag{36}$$

Equations (36) are solved for $\omega_{n_1}^2$, $\omega_{n_2}^2$, $\lambda_1$, $\lambda_2$ and $\sqrt{\mu_1\mu_2}$, using the least square fit technique. The joint probability function, $p(x_1, x_2)$ and variances, $\sigma_{\dot{x}_1}^2$ and $\sigma_{\dot{x}_2}^2$, are computed from the experimentally obtained displacement and velocity data ($x_1$, $x_2$, $\dot{x}_1$ and $\dot{x}_2$), which are taken as zero mean Gaussian processes, and the non-linear spring force provided by the rolling element bearings is taken to be cubic in nature; i.e., $G(x) = x^3$. The stiffness matrix definition for the three body lumped parameter shaft model (Figure 1) is as follows [21]:

$$[K]=m_3\begin{bmatrix}\omega_{11}^2 & \omega_{13}^2 & \omega_{12}^2\\ \omega_{31}^2 & \omega_{33}^2 & \omega_{32}^2\\ \omega_{21}^2 & \omega_{23}^2 & \omega_{22}^2\end{bmatrix}=\frac{12EI}{L^3}\begin{bmatrix}1 & -1 & 0\\ -1 & 2 & -1\\ 0 & -1 & 1\end{bmatrix}. \tag{37}$$

The laboratory rig for the experimental illustration of the technique is shown in Figures 2 and 3. The rig consists of a disc centrally mounted on a shaft supported in two ball bearings. The shaft is driven through a flexible coupling by a motor and the vibration signals are picked up (after balancing the rotor) in both the vertical and horizontal directions by accelerometers mounted on both of the bearing housings. The signals from the accelerometers are digitized on a PC/AT after magnification.

Typical displacement and velocity signals, in the vertical direction, picked up by the accelerometer are given in Figures 4–7. The joint probability density function, $p(x_1, x_2)$,

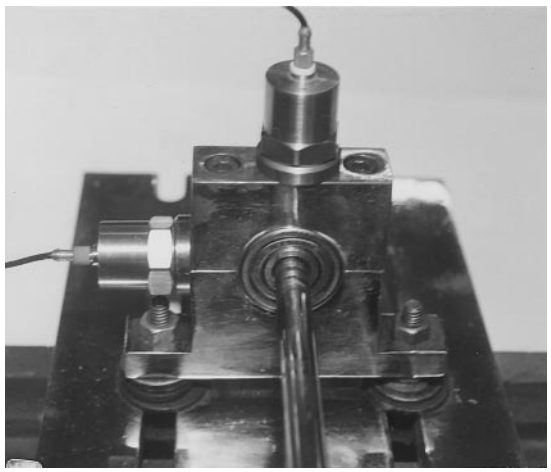

Figure 3. The accelerometer locations.

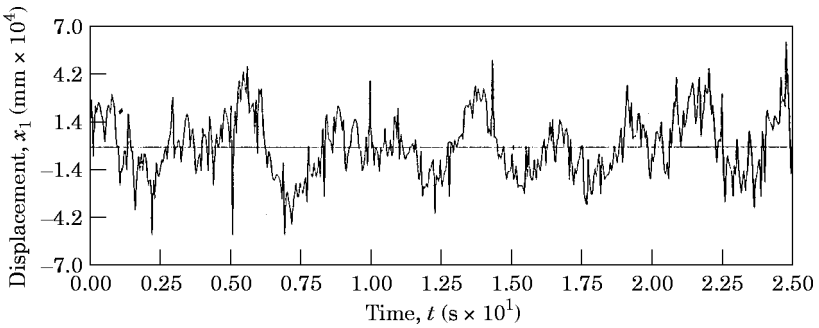


Figure 4. The displacement signal in the vertical direction at bearing 1.

of the displacements is shown in Figure 8. The bearing parameters estimated from equations (36), with the following set of data, $EI = 1{\cdot}03 \times 10^8$ N mm$^2$, $m_3 = 0{\cdot}515$ kg, $L = 250{\cdot}0$ mm, are given in Table 1. Bearing stiffness parameters estimated for the horizontal direction are also given in this table, along with those estimated for the vertical direction. The analysis in the horizontal direction remains similar to that in the vertical direction and the horizontal parameters are obtained from the horizontal displacement and the velocity signals; i.e., ($y_1$, $y_2$, $\dot{y}_1$, $\dot{y}_2$) from equations similar to equations (36).

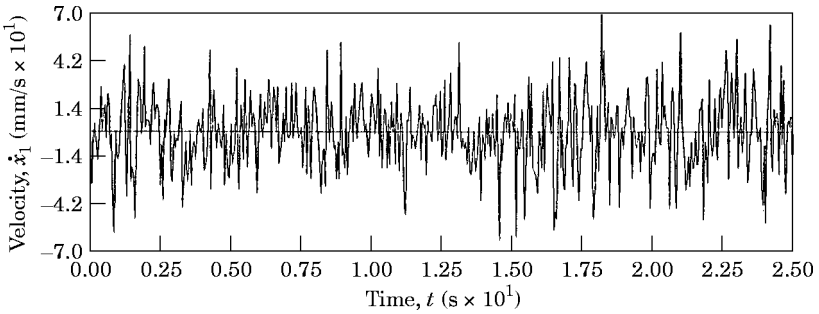


Figure 5. The velocity signal in the vertical direction at bearing 1.

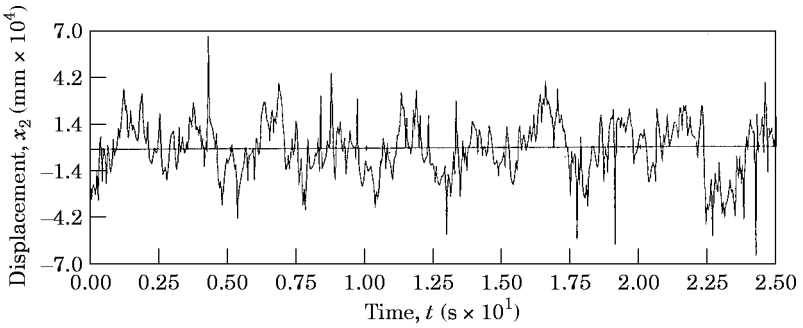


Figure 6. The displacement signal in the vertical direction at bearing 2.

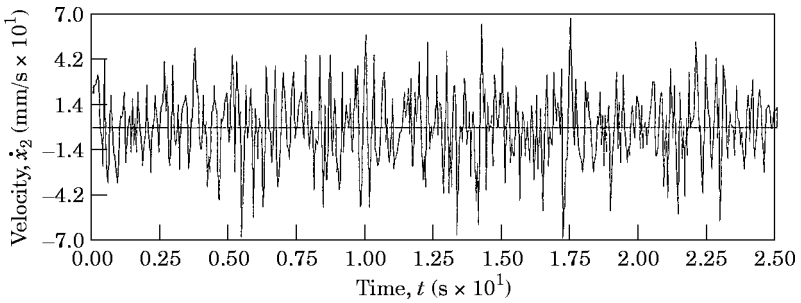


Figure 7. The velocity signal in the vertical direction at bearing 2.

## 5. SIMULATION

The algorithm is tested by Monte Carlo simulation. The experimentally obtained values of $\omega_{n_1}^2$, $\omega_{n_2}^2$, $\lambda_1$, $\lambda_2$ and $\sqrt{\mu_1\mu_2}$ are used in equation (8) to simulate the displacement and velocity responses, $x_1$, $x_2$, $\dot{x}_1$ and $\dot{x}_2$, through the fourth order Runga–Kutta numerical technique, for broad-band excitation forces, $f_1(t)$ and $f_2(t)$, with zero mean and Gaussian probability distribution as described in Figures 9–12. The vertical displacement and velocity responses resulting at the two bearings due to the simulated forces of Figures 9–12 are given in Figures 13–16. The joint probability distribution of the simulated vertical displacements is shown in Figure 17. The simulated response is now fed into equation (36)

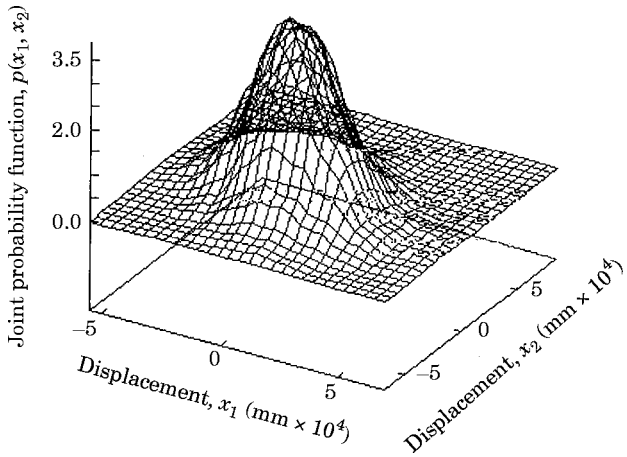


Figure 8. The joint probability density distribution of vertical displacements at bearing 1 and bearing 2.

TABLE 1

*Experimental bearing stiffness and mass parameters*

| Parameters | Vertical | Horizontal |
|---|---|---|
| $\omega_{n_1}^2$ (rad/s)$^2$ | $2{\cdot}13 \times 10^7$ | $2{\cdot}12 \times 10^7$ |
| $\lambda_1$ (mm)$^{-2}$ | $-1{\cdot}25 \times 10^6$ | $-1{\cdot}41 \times 10^6$ |
| $\omega_{n_2}^2$ (rad/s)$^2$ | $1{\cdot}98 \times 10^7$ | $2{\cdot}21 \times 10^7$ |
| $\lambda_2$ (mm)$^{-2}$ | $-1{\cdot}15 \times 10^6$ | $-1{\cdot}36 \times 10^6$ |
| $\sqrt{\mu_1\mu_2}$ | 2·10 | 2·34 |

to obtain the values of $\omega_{n_1}^2$, $\omega_{n_2}^2$, $\lambda_1$, $\lambda_2$ and $\sqrt{\mu_1\mu_2}$. A similar exercise is carried out to obtain the parameters in the horizontal direction. These values are listed in Table 2.

The good agreement between the values of the bearing stiffness parameters, $\omega_{n_1}^2$, $\omega_{n_2}^2$, $\lambda_1$, $\lambda_2$ and $\sqrt{\mu_1\mu_2}$, obtained by processing the experimental data and those from the Monte Carlo simulation, indicates the correctness of the experimental and algebraic exercises. It should be noted that the simulated values of the bearing stiffness parameters are obtained for an ideal white noise excitation, while the experimental ones are obtained by processing the actual response of the system, where the unknown excitation was idealized as white noise. It also needs to be pointed out that the values of the damping parameters $\alpha_{ij}$, are not required for the estimation procedure (equation (36)). Any convenient set of values of $\alpha_{ij}$ can be employed in equations (8)–(10) for the purpose of simulation.

## 6. VALIDATION

The values of the bearing stiffness parameters $\omega_n^2$ and $\lambda$, obtained by the procedure outlined, are compared with those obtained from the analytical formulations of Harris [7]

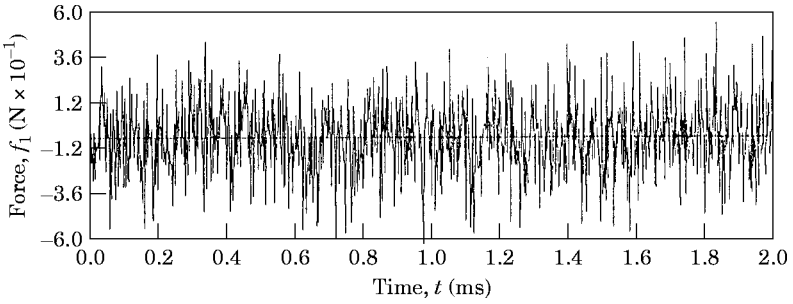


Figure 9. The simulated random force at bearing 1.

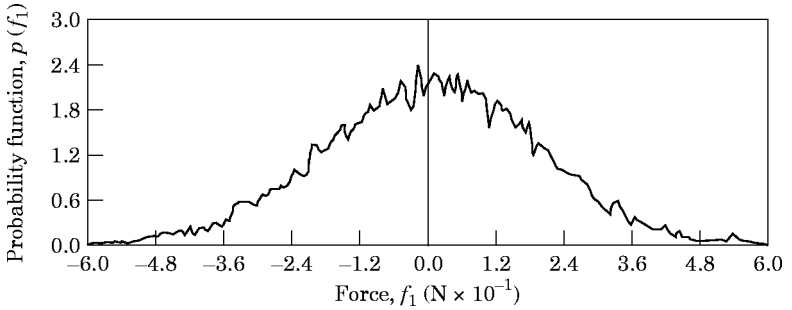


Figure 10. The probability density distribution of the simulated force at bearing 1.

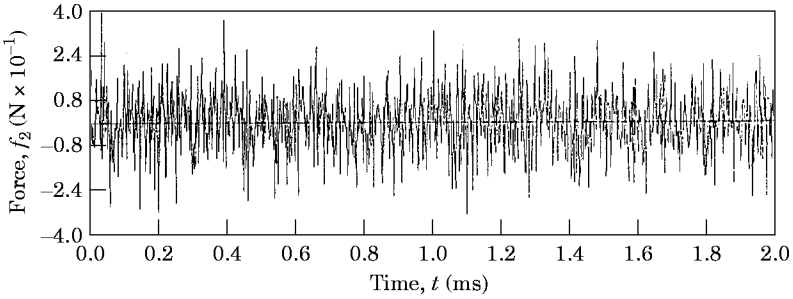


Figure 11. The simulated random force at bearing 2.

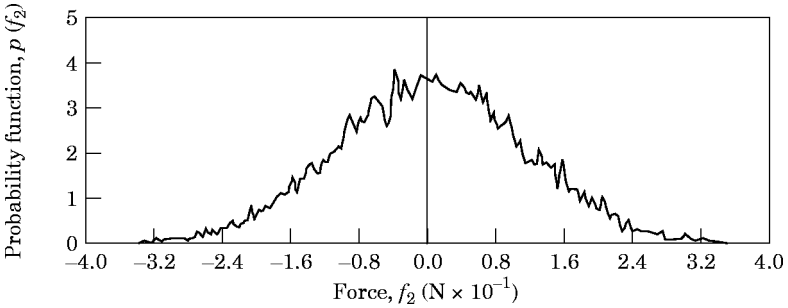


Figure 12. The probability density distribution of the simulated force at bearing 2.

and Ragulskis [6], which are based on Hertzian contact theory. The total elastic force at the points of contact of the $i$th ball with the inner and outer races is expressed as [6]

$$F_i = K_n(g + x\cos\eta_i + y\sin\eta_i)^{3/2} \tag{38}$$

and its projection along the line of action of the applied force is

$$F_i = K_n(g + x\cos\eta_i + y\sin\eta_i)^{3/2}\cos\eta_i, \tag{39}$$

where $g$ is the radial preload or preclearance between the ball and the races, and $x$ and $y$ are the displacements of the moving ring in the direction of the radial load and perpendicular to the direction of the radial load respectively. $\eta_i$ is the angle between the lines of action of the radial load (direction of displacement of the moving ring) and the radius passing through the center of the $i$th ball. $K_n$ is a coefficient of proportionality depending on the geometric and material properties of the bearing. The specifications of the two test bearings are as follows: ball bearing type, SKF 6200; number of balls, six;

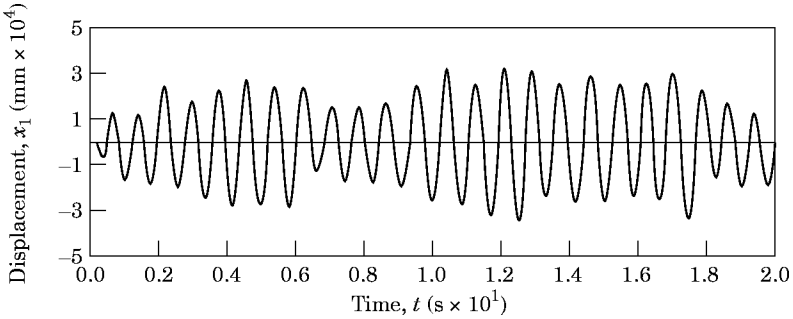


Figure 13. The simulated displacement signal at bearing 1.

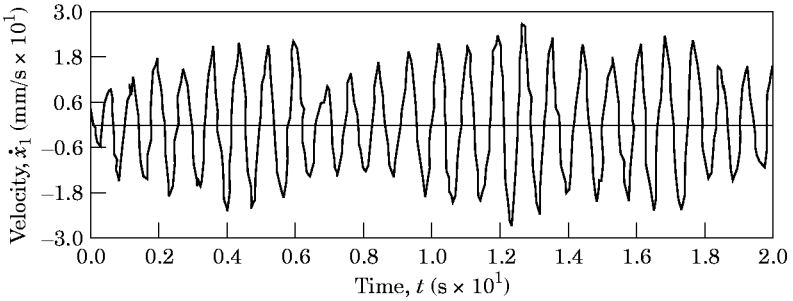


Figure 14. The simulated velocity signal at bearing 1.

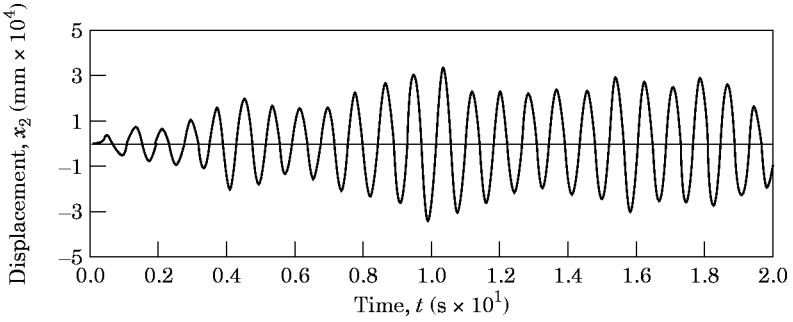


Figure 15. The simulated displacement signal at bearing 2.

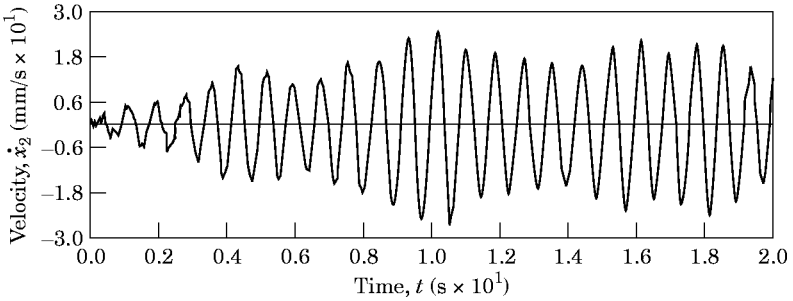


Figure 16. The simulated velocity signal at bearing 2.

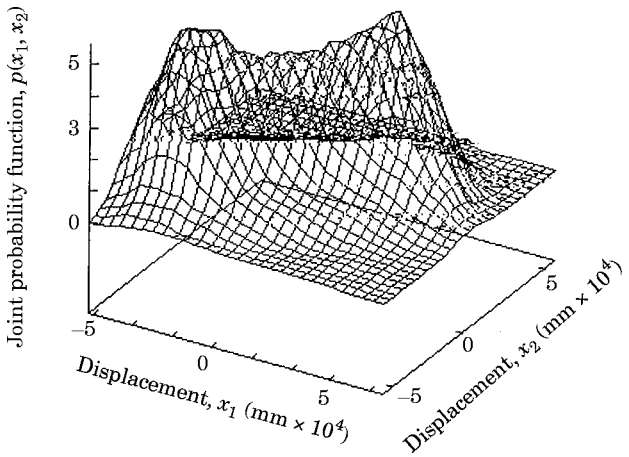


Figure 17. The joint probability density distribution.

TABLE 2

*Experimental and simulated bearing stiffness and mass parameters*

| | Vertical | | Horizontal | |
|---|---|---|---|---|
| Parameters | Experimental | Simulated | Experimental | Simulated |
| $\omega_{n_i}^2$ (rad/s)$^2$ | $2{\cdot}13 \times 10^7$ | $2{\cdot}12 \times 10^7$ | $2{\cdot}11 \times 10^7$ | $2{\cdot}21 \times 10^7$ |
| $\lambda_1$ (mm)$^{-2}$ | $-1{\cdot}25 \times 10^6$ | $-1{\cdot}41 \times 10^6$ | $-1{\cdot}29 \times 19^6$ | $-1{\cdot}45 \times 10^6$ |
| $\omega_{n_2}^2$ (rad/s)$^2$ | $1{\cdot}98 \times 10^7$ | $2{\cdot}21 \times 10^7$ | $1{\cdot}95 \times 10^7$ | $2{\cdot}23 \times 10^7$ |
| $\lambda_2$ (mm)$^{-2}$ | $-1{\cdot}15 \times 10^6$ | $-1{\cdot}36 \times 10^6$ | $-1{\cdot}63 \times 10^6$ | $-1{\cdot}86 \times 10^6$ |
| $\sqrt{\mu_1 \mu_2}$ | 2·10 | 2·43 | 2·34 | 2·50 |

ball diameter, 6 mm; bore diameter, 10 mm; outer diameter, 30 mm; pitch diameter, 20 mm; groove radius, 3·09 mm; allowable pre-load, 0–2 $\mu$m. The value of $K_n$, for the test bearing with the above specifications, is estimated by the method suggested by Harris [7] as $2{\cdot}82 \times 10^5$ N/mm$^{1{\cdot}5}$.

The total elastic force in the direction of the applied force is

$$F = \sum_{i=1}^{n} F_i, \tag{40}$$

where $n$ is the total number of balls in the bearing. Using the condition of zero elastic force in the direction perpendicular to the elastic load, the deformation, $y$, perpendicular to the radial force line is expressed as

$$y = \sum_{i=1}^{n} [g + x \cos(\eta_i)]^{3/2} \sin(\eta_i) \Big/ \sum_{i=1}^{n} [g + x \cos(\eta_i)]^{1/2} \sin^2(\eta_i). \tag{41}$$

Equations (39) and (41) are used in equation (40) and the bearing stiffness is determined as a function of the deformation $x$ as

$$k(x) = \partial F / \partial x. \tag{42}$$

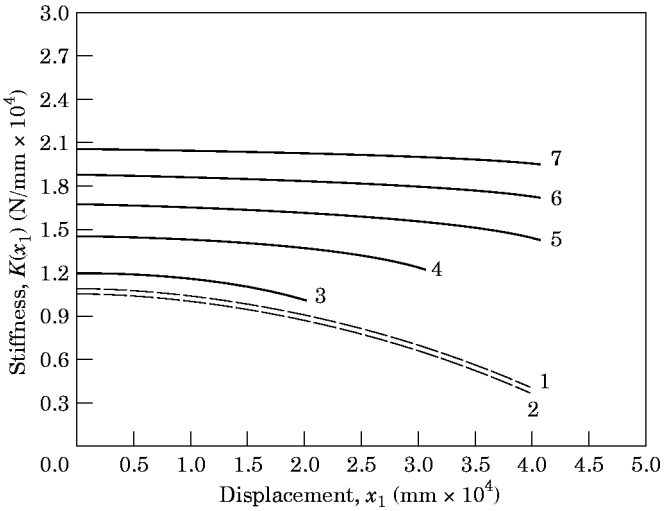


Figure 18. A comparison of the rolling element bearing stiffnesses at bearing 1.

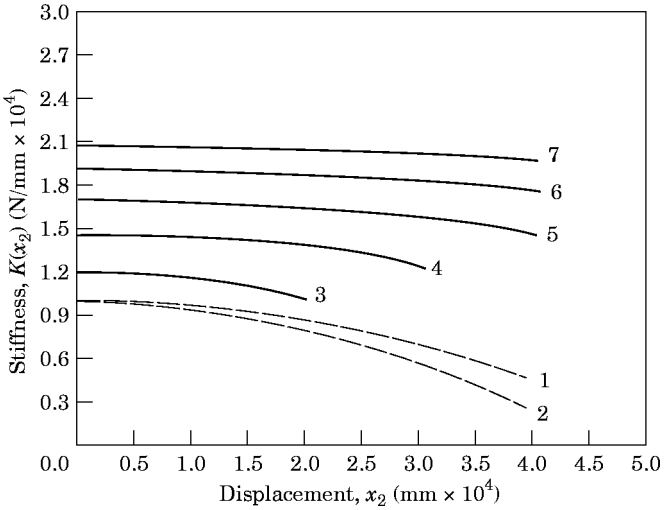


Figure 19. A comparison of the rolling element bearing stiffnesses at bearing 2.

It can be seen that the bearing stiffness is critically dependent on the pre-loading, $g$, of the balls. While the manufacturer may, at times, provide the pre-load range, the exact value of the pre-loading of the bearing balls in the shaft–casing assembly, especially during operations which have involved wear and tear, would be difficult to determine. The stiffness of the test bearing is plotted in Figures 18 and 19 as a function of the radial deformation, $x$, for various allowable preload values, $g$. The bearing stiffness obtained experimentally, using the procedure developed, also shown in Figures 18 and 19, shows good resemblance to theoretically possible values. It is also to be noted that the theoretical stiffness calculations are based on formulations which analyze the bearing in isolation of the shaft. The comparison between the experimental and theoretically possible stiffness is also listed in Table 3. The expressions for the theoretical stiffness in Table 3 have been obtained by curve fitting the stiffness values obtained from equation (36), through a quadratic in $x$.

In an earlier analysis by the authors [19], where the shaft flexibility was not accounted for and was treated as a rigid body, and the analysis was restricted to a single-degree-of-freedom idealization, the bearing stiffness for the same experimental set-up was found to be $1{\cdot}32 \times 10^4$–$5{\cdot}08 \times 10^{10}x^2$ (N/mm) and $2{\cdot}23 \times 10^4$–$8{\cdot}50 \times 10^{10}x^2$

TABLE 3

*Experimental and theoretical* [6, 7] *bearing stiffness parameters*

| Preload (mm) | Theoretical stiffness (radial) (N/mm) | Experimental stiffness (N/mm) (at bearing 1) | Experimental stiffness (N/mm) (at bearing 2) |
|---|---|---|---|
| 0·0002 | $1{\cdot}20 \times 10^4$–$4{\cdot}01 \times 10^{10}x^2$ | | |
| | | $1{\cdot}08 \times 10^4$–$4{\cdot}19 \times 10^{10}x^2$ (horizontal) | $1{\cdot}01 \times 10^4$–$4{\cdot}91 \times 10^{10}x^2$ (horizontal) |
| 0·0003 | $1{\cdot}47 \times 10^4$–$2{\cdot}18 \times 10^{10}x^2$ | | |
| 0·0004 | $1{\cdot}69 \times 10^4$–$1{\cdot}42 \times 10^{10}x^2$ | | |
| 0·0005 | $1{\cdot}89 \times 10^4$–$1{\cdot}02 \times 10^{10}x^2$ | | |
| | | $1{\cdot}10 \times 10^4$–$4{\cdot}13 \times 10^{10}x^2$ (vertical) | $1{\cdot}02 \times 10^4$–$3{\cdot}52 \times 10^{10}x^2$ (vertical) |
| 0·0006 | $2{\cdot}08 \times 10^4$–$6{\cdot}09 \times 10^9x^2$ | | |

(N/mm) in the horizontal and vertical directions respectively. A comparison with the stiffness values of Table 3 reveals the influence of shaft flexibility.

While good agreement on the bearing stiffness parameters is observed between the values generated following the method of Harris and Ragulskis [6, 7] and those obtained experimentally through the present procedure, the values of the effective masses at the bearing ends, obtained as by-products of the present procedure, also look reasonable. The experimentally obtained values of $\sqrt{\mu_1 \mu_2}$ are 2·1 and 2·34 (Table 1) in the vertical and horizontal directions respectively. If the two bearings are taken to be identical, the effective mass computed (knowing that the disc mass is 0·515 kg) for each of the bearing ends turns out to be 0·245 kg in the vertical direction and 0·220 kg in the horizontal direction. These values look reasonable, in view of the fact that along with some contribution from the bearings themselves, a division of the mass of the shaft, which in this case is 0·306 kg, is seen at the two bearing ends.

## 7. CONCLUSIONS

The procedure outlined for estimation of linear and non-linear bearing stiffness parameters from random response in flexible rotors, although developed for a shaft carrying a single disc, can be readily employed for shafts with multiple discs. While making certain engineering approximations, of idealizing the excitations from bearing surface and assembly imperfections as white noise sources, the procedure holds a distinct advantage over other available techniques, in that it does not involve estimation of the excitation forces and works directly on the random response signals which can be conveniently picked up at the rotor–bearing caps.

## REFERENCES

1. H. Hertz 1986 *Miscellaneous Papers*, 163–183. London: Macmillan. On the contact of rigid elastic solids and on hardness.
2. G. Lohman 1953 *Konstruktion* **5**. Untersuchung des Laufgerausches von Walzlgern.
3. O. Gustavsson and T. Tallian 1962 *Transactions of the American Society of Locomotive Engineers* **5**. Detection of damage in assembled rolling element bearings.
4. K. Honrath 1960 *Thesis submitted for Dicktor Ingenieur at the Technical University of Aachen*. Concerning the stiffness of machine tool spindles and their bearings.
5. M. Elsermans, M. Hongerloot and R. Snoeys 1975 *Proceedings of the* 16*th MTDR Conference*, Manchester, 10–12 September, 223. Damping in taper rolling bearings.
6. K. M. Ragulskis, A. Yu. Jurkauskas, V. V. Atastupenas, A. Yu. Vitkute and A. P. Kulvec 1974 *Vibrations of Bearings*. Vilnyus: Mintis Publishers.
7. T. A. Harris 1984 *Rolling Bearing Analysis*. New York: John Wiley.
8. V. O. Kononenko and N. P. Plakhtienko 1970 *Prikladnaya Mekhanika* **6**, Vyp. 9. Determination of nonlinear vibration system characteristics from analysis of vibrations.
9. T. L. H. Walford and B. J. Stone 1980 *Journal of Mechanical Engineering Science* **22**(4), 175–181. The measurement of the radial stiffness of rolling element bearings under oscillation conditions.
10. P. D. McFadden and J. D. Smith 1984 *International Journal of Tribology* **17**, 3–10. Vibration monitoring of rolling element bearings by the high-frequency resonance technique—a review.
11. C. S. Sunnersjo 1985 *Journal of Sound and Vibration* **98**, 455–474. Rolling bearing vibrations—the effects of geometrical imperfections and wear.
12. P. D. McFadden and J. D. Smith 1985 *Journal of Sound and Vibration* **98**, 263–273. The vibration produced by multiple point defects in a rolling element bearing.
13. Y. T. Su, M. H. Lin and M. S. Lee 1993 *Journal of Sound and Vibration* **165**, 455–466. The effects of surface irregularities on roller bearing vibrations.
14. J. Kraus, J. J. Blech and S. G. Braun 1987 *Transaction of American Society of Mechanical*

*Engineers*, *Journal of Vibration*, *Acoustics*, *Stress*, *and Reliability in Design* **109**, 235–240. In situ determination of rolling bearing stiffness and damping by modal analysis.
15. A. Muszynska and D. E. Bently 1990 *Journal of Sound and Vibration* **143**, 103–124. Frequency-swept rotating input perturbation techniques and identification of the fluid force models in rotor/bearing/seal systems and fluid handling machines.
16. M. J. Goodwin 1991 *Transaction of the American Society of Mechanical Engineers*, *Journal of Engineering for Industry* **113**, 335–342. Experimental techniques for bearing impedance measurement.
17. D. P. Hess, A. Soom and C. H. Kim 1992 *Journal of Sound and Vibration* **153**, 491–508. Normal vibrations and friction at a Hertzian contact under random excitation: theory and experiments.
18. T. C. Lim and R. Singh 1994 *Journal of Sound and Vibration* **169**, 547–553. Vibration transmission through rolling element bearings, part V: effect of distributed contact load on roller bearing stiffness matrix.
19. R. Tiwari and N. S. Vyas 1995 *Journal of Sound and Vibration* **187**, 229–239. Estimation of nonlinear stiffness parameters of rolling element bearings from random response of rotor bearing systems.
20. J. S. Rao 1966 *Rotor Dynamics*. New Delhi: Wiley Eastern Limited.
21. D. Childs 1993 *Turbomachinery Rotordynamics: Phenomena*, *Modeling and Analysis*. New York: Wiley-Interscience.
22. H. D. Nelson, W. L. Meacham, D. P. Fleming and A. F. Kascak 1983 *Transactions of the American Society of Mechanical Engineers*, *Journal of Engineering for Power* **105**, 606–614, Nonlinear analysis of rotor–bearing systems using component mode synthesis.
23. N. C. Nigam 1983 *Introduction To Random Vibrations*. Cambridge, MA: The MIT Press.
24. Y. K. Lin 1973 *Stochastic Problems in Mechanics*. Study No. 10, Solid Mechanics Division, University of Waterloo, Stochastic aspects of dynamic systems.
25. T. K. Caughey 1963 *Journal of the Acoustical Society of America* **35**(11), 1683–1692. Derivation and application of the Fokker–Planck equation to discrete nonlinear dynamic systems subjected to white random excitation.
26. J. B. Roberts and P. D. Spanos 1990 *Random Vibration and Statistical Linearization*. New York: John Wiley.

## APPENDIX A: EIGENVALUES AND EIGENVECTORS

Eigen values:

$$p_1^2 = 0,$$

$$p_{2,3}^2 =$$

$$\left[\frac{12EI}{m_3L^3}\right]\frac{m_1m_3+2m_1m_2+m_2m_3 \mp \sqrt{-4m_1m_2m_3(m_1+m_2+m_3)+(m_1m_3+2m_1m_2+m_2m_3)^2}}{2m_1m_2m_3}.$$

Eigen vectors:

$$U = \begin{bmatrix} 1 & u_{31} & u_{21} \\ 1 & u_{32} & u_{22} \\ 1 & 1 & 1 \end{bmatrix},$$

with

$$u_{21} = -1 + \frac{1}{4m_1^2m_2m_3}[\{m_1m_3 - 2m_1m_2 - m_2m_3 + \sqrt{m_1^2m_3^2 - 2m_1m_2m_3^2 + 4m_1^2m_2^2 + m_2^2m_3^2}\} \times \{-m_1m_3 + 2m_1m_2 - m_2m_3 + \sqrt{m_1^2m_3^2 - 2m_1m_2m_3^2 + 4m_1^2m_2^2 + m_2^2m_3^2}\}],$$

$$u_{22} = \frac{\{m_1m_3 - 2m_1m_2 - m_2m_3 + \sqrt{m_1^2m_3^2 - 2m_1m_2m_3^2 + 4m_1^2m_2^2 + m_2^2m_3^2}\}}{2m_1m_3},$$

$$u_{31} = -1 + \frac{1}{4m_1^2m_2m_3}[\{m_1m_3 - 2m_1m_2 - m_2m_3 - \sqrt{m_1^2m_3^2 - 2m_1m_2m_3^2 + 4m_1^2m_2^2 + m_2^2m_3^2}\} \times \{-m_1m_3 + 2m_1m_2 - m_2m_3 - \sqrt{m_1^2m_3^2 - 2m_1m_2m_3^2 + 4m_1^2m_2^2 + m_2^2m_3^2}\}].$$

$$u_{32} = \frac{\{m_1m_3 - 2m_1m_2 - m_2m_3 + \sqrt{m_1^2m_3^2 - 2m_1m_2m_3^2 + 4m_1^2m_2^2 + m_2^2m_3^2}\}}{2m_1m_3},$$

## APPENDIX B: NOMENCLATURE

| | | | |
|---|---|---|---|
| $c_1, c_2, c_3$ | normalization constants | $u_{ij}$ | eigenvector elements |
| $F_i$ | random excitation force | $x, y, z$ | rectangular co-ordinate system |
| $F_b$ | bearing force | $x, \dot{x}, \ddot{x}$ | displacement, velocity and acceleration, respectively |
| $F_d$ | shaft damping force | | |
| $F_s$ | shaft stiffness force | $t$ | time |
| $g$ | pre-load on the rolling elements | $V(x)$ | potential energy term |
| $g(x), G(x)$ | non-linear functions | $\alpha_{ij}$ | shaft damping parameter |
| $k_L, k_{NL}$ | linear and non-linear stiffness parameters of bearings | $\eta_i$ | generalized co-ordinates |
| | | $\phi_i$ | random excitation intensity factor |
| $k_{ij}$ | shaft stiffness parameter | $\gamma$ | $= \beta/m\phi$, ratio |
| $k(x)$ | $= k_L + k_{NL}x^2$, bearing non-linear stiffness | $\lambda$ | $= k_{NL_i}/\omega_{n_i}^2 m_3$, non-linear stiffness contribution parameter |
| $K_n$ | coefficient of proportionality | $\mu_i$ | disc mass to effective bearing mass ratio |
| $m_1, m_2$ | effective bearing masses | | |
| $m_3$ | disc mass | $\omega_{ij}^2$ | $= k_{ij}/m_3$, shaft stiffness parameter |
| $N$ | number of sample points | $\omega_{n_{ij}}^2$ | $= k_{L_i}/m_3$, bearing linear stiffness parameter |
| $p(x), p(\dot{x})$ | probability density functions of displacement and velocity, respectively | $\sigma_{\dot{x}}^2$ | variance of velocity |